Numerical Simulation of ATPS Parachute Transient Dynamics Using Fluid-Structure Interaction Method

Fan Yuxin, *Xia Jian**

College of Aerospace Engineering, Nanjing University of Aeronautics and Astronautics, Nanjing 210016, P. R. China

(Received 15 February 2015; revised 23 June 2015; accepted 1 July 2015)

Abstract: In order to simulate and analyze the dynamic characteristics of the parachute from advanced tactical parachute system (ATPS), a nonlinear finite element algorithm and a preconditioning finite volume method are employed and developed to construct three dimensional parachute fluid-structure interaction (FSI) model. Parachute fabric material is represented by membrane-cable elements, and geometrical nonlinear algorithm is employed with wrinkling technique embedded to simulate the large deformations of parachute structure by applying the Newton-Raphson iteration method. On the other hand, the time-dependent flow surrounding parachute canopy is simulated using preconditioned lower-upper symmetric Gauss-Seidel (LU-SGS) method. The pseudo solid dynamic mesh algorithm is employed to update the flow-field mesh based on the complex and arbitrary motion of parachute canopy. Due to the large amount of computation during the FSI simulation, massage passing interface(MPI) parallel computation technique is used for all those three modules to improve the performance of the FSI code. The FSI method is tested to simulate one kind of ATPS parachutes to predict the parachute configuration and anticipate the parachute descent speeds. The comparison of results between the proposed method and those in literatures demonstrates the method to be a useful tool for parachute designers.

Key words: parachute dynamics; fluid-structure interaction; nonlinear structure dynamics; time dependent flow; parallel computation technique

CLC number: V244.21 **Document code**: A **Article ID**: 1005-1120(2017)05-0535-08

0 Introduction

Although parachute system is the most useful air-dropping device, it brings many challenges for both experimental test and numerical simulation[1]. Moreover, the modern combat-ready airborne troops are usually equipped with heavier tactical weapons and need more slowly impact speed at the end of parachute landing procedure. Designing new parachute configurations such as advanced tactical parachute system (ATPS) parachute program will need more convenient numerical method to predict and evaluate parachute dynamic characteristics.

One kind of parachute fluid-structure interaction (FSI) method uses mass-spring damper (MSD) model to treat the parachute as a virtual spring net. Although this spring model can provide basic parachute profiles[2-5] or shapes[6] for fluid computation, it is still difficult to simulate complex new parachute configurations especially when the strings go through the fabric canopy. The other kind of parachute FSI method is the deforming-spatial-domain/stabilized space-time (DSD/SST) formulation[7-13] which is based on finite element method. However, using finite element method to solve flow problem can be very time-consuming and need extra technique to solve compressible flow problems. The last kind of parachute FSI method is using commercial software[14-15], but they usually use explicit iteration method which can severely limit time step.

A FORTRAN code containing three modules is developed within massage passing interface

* Corresponding author, E-mail address: jxia@nuaa.edu.cn.

How to cite this article: Fan Yuxin, Xia Jian. Numerical simulation of ATPS parachute transient dynamics using fluid-structure interaction method[J]. Trans. Nanjing Univ. Aero. Astro., 2017,34(5):535-542.
http://dx.doi.org/10.16356/j.1005-1120.2017.05.535

(MPI) parallel environment in this paper to conduct the FSI simulation of ATPS parachute problems. The three modules are implicit nonlinear finite element structure solver, preconditioned unsteady flow solver and pseudo solid dynamic mesh solver, respectively. The FSI method combines the implicit nonlinear structure dynamic algorithm with the unsteady preconditioning method for the first time to predict ATPS parachute dynamic characteristics. The simulation results agree with Ref. [1], which demonstrates its ability in helping design new parachute configurations.

1 Nonlinear Structure Dynamic Model

1.1 Governing equation for structure model

The nonlinear structure dynamic formula for membrane-cable system can be established by applying total Lagrangian scheme with incremental/iteration method[16, 17]

$$\boldsymbol{M}\cdot{}_{k+1}^{t+\Delta t}\ddot{\boldsymbol{U}}+\boldsymbol{C}\cdot{}_{k+1}^{t+\Delta t}\dot{\boldsymbol{U}}+{}_{k}^{t+\Delta t}\boldsymbol{K}_{\mathrm{T}}\cdot\left[{}_{k+1}^{t+\Delta t}\boldsymbol{U}-{}_{k}^{t+\Delta t}\boldsymbol{U}\right]={}_{k+1}^{t+\Delta t}\boldsymbol{F}-{}_{k}^{t+\Delta t}\boldsymbol{R} \tag{1}$$

where $\boldsymbol{M}$, $\boldsymbol{C}$, $\boldsymbol{K}_{\mathrm{T}}$ and $\boldsymbol{U}$ are consistent mass matrix, mass damping matrix, tangent stiffness matrix, global displacements vector, respectively. $\boldsymbol{F}$ and $\boldsymbol{R}$ are the pressure loading and the restoring force, respectively. The superscript t represents structural time step and the corresponding subscript k the Newton-Raphson iteration number. The second Piola-Kirchoff stress tensor $\boldsymbol{S}^{\alpha\beta}$ and Green-Lagrange strain tensor $\boldsymbol{E}^{\xi\eta}$ are employed to describe the geometrical nonlinear deformation system based on the fourth-order elastic tensor $\boldsymbol{C}_{\alpha\beta\,\xi\eta}$

$$\boldsymbol{S}^{\alpha\beta}=\boldsymbol{C}_{\alpha\beta\xi\eta}\boldsymbol{E}^{\xi\eta} \tag{2}$$

The membrane tangent stiffness matrix $\boldsymbol{K}$ for nonlinear structural simulation is[17]

$$\begin{aligned}{}_{k}^{t+\Delta t}\boldsymbol{K}_{N_iM_j}=&\frac{1}{2}\delta_{ij}\boldsymbol{S}^{\alpha\beta}(H_{N,\alpha}H_{M,\beta}+H_{M,\alpha}H_{N,\beta})h\sqrt{\boldsymbol{G}}+\frac{1}{4}\boldsymbol{C}_{\alpha\beta\xi\eta}\cdot(H_{N,\alpha}H_{L,\beta}+H_{L,\alpha}H_{N,\beta})\cdot(X_{Li}+{}_{k}^{t+\Delta t}U_{Li})(H_{M,\xi}H_{Q,\eta}+\\&H_{Q,\xi}H_{M,\eta})(X_{Qj}+{}_{k}^{t+\Delta t}U_{Qj})\cdot h\sqrt{\boldsymbol{G}}\end{aligned} \tag{3}$$

where $\boldsymbol{G}$ is the metric tensor; h the membrane thickness; δ the Kronecker symbol. N, M, L, Q are the local node index of one element; i, j the three directions of Cartesian coordinates; Capital letter X and H the Cartesian coordinates and interpolation shape function, respectively. Similarly, the tangent stiffness matrix for the nonlinear cable elements is (A_s represents cable cross-sectional area)

$$\begin{aligned}{}_{k}^{t+\Delta t}\boldsymbol{K}_{N_iM_j}=&\delta_{ij}\boldsymbol{S}^{11}H_{N,1}H_{M,1}A_s\sqrt{\boldsymbol{G}}+\\&EA^{11}A^{11}H_{N,1}H_{L,1}\cdot(X_{L_i}+{}_{k}^{t+\Delta t}U_{L_i})\cdot\\&H_{M,1}H_{Q,1}\cdot(X_{Q_j}+{}_{k}^{t+\Delta t}U_{Q_j})A_s\sqrt{\boldsymbol{G}}\end{aligned} \tag{4}$$

It should be noticed that the membrane wrinkling algorithm in Ref. [18] is employed in this paper to eliminate the compression stress in the membrane elements, which can simulate the fabric special wrinkling phenomenon and improve the numerical stability.

1.2 Structural time-integration formulation

By applying the implicit Newmark time integration scheme[17], the structural dynamic equation at time level $t+\Delta t$ with nonlinear Newton-Raphson iteration step number k is

$$\begin{aligned}&\left[{}_{k}^{t+\Delta t}\boldsymbol{K}_{\mathrm{T}}+\frac{M}{\beta\Delta t^2}+\frac{\alpha}{\beta\Delta t}C\right]\left[{}_{k+1}^{t+\Delta t}\boldsymbol{U}-{}^{t}\boldsymbol{U}\right]=\\&{}_{k+1}^{t+\Delta t}\boldsymbol{F}-{}_{k}^{t+\Delta t}\boldsymbol{R}-\boldsymbol{M}\cdot\left\{\frac{1}{\beta\Delta t^2}\left[{}_{k}^{t+\Delta t}\boldsymbol{U}-{}^{t}\boldsymbol{U}\right]-\frac{\dot{\boldsymbol{U}}}{\beta\Delta t}-\left(\frac{1}{2\beta}-1\right)\cdot{}^{t}\ddot{\boldsymbol{U}}\right\}-\boldsymbol{C}\cdot\left\{\left(1-\frac{\alpha}{\beta}\right)\cdot\right.\\&\left.{}^{t}\boldsymbol{U}+\Delta t\left(1-\frac{\alpha}{2\beta}\right)\cdot{}^{t}\ddot{\boldsymbol{U}}+\frac{\alpha}{\beta\Delta t}\left[{}_{k}^{t+\Delta t}\boldsymbol{U}-{}^{t}\boldsymbol{U}\right]\right\}\end{aligned} \tag{5}$$

where α and β are chosen as 0.500 and 0.250, respectively. The generalized minimal residual (GMRES)[19] iteration algorithm is used in this paper to solve these large scale nonlinear structural dynamic equations because of its fast convergence and robust characteristics.

1.3 Structural parallel computation strategy

The nonlinear structural algorithm mainly contains two numerical operating levels[16]: Element and system level. The element level uses structural elements and their local nodes to assemble tangent stiffness matrix or force vector, while the system level uses the system nodes to conduct matrix-vector multiplication. Based on these basic numerical operating characteristics, a parallel computation technique is designed here based on the MPI library functions MPI_IRecv

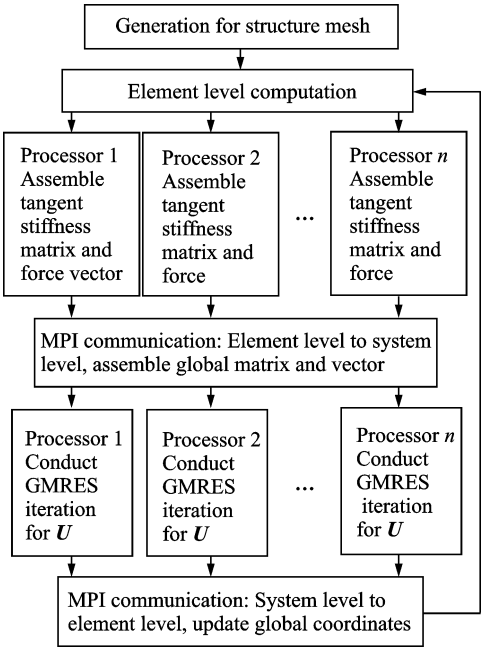

Fig. 1 Structural parallel computation procedure

and MPI_ISend, as shown in Fig. 1.

1.4 Verification of parallel structural method

The test case is the classical air bag inflation problem. The membrane thickness is 3.048×10^{-5} m and the edge length is 0.304 8 m. It is inflated by a constant pressure 23.94 Pa[18]. The Young's modulus is 206.8 MPa and the Poisson ratio is 0.30. The time step is 1.0×10^{-4} s and the inflation time is 0.05 s. The partition is made by calling the library functions provided by open source code METIS, which uses node connective relationship to generate balanced logical partition results.

MPI partition result of the initial state is demonstrated in Fig. 2(a). The displacements of numerical simulation (Figs. 2(b, c)) in both the in-plane and transverse directions agree well with those in Ref. [18].

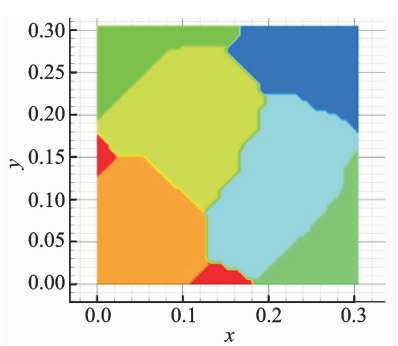

(a) MPI partition result of initial configuration

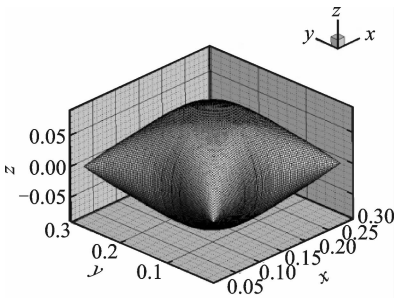

(b) Numerical inflation results (side view)

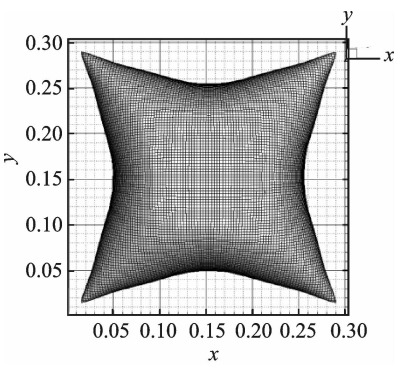

(c) Numerical inflation results (top view)

Fig. 2 Air bag inflation case

The structural parallel computation efficiency is demonstrated in Table 1, where the efficiency is defined as the processor number divided by the ratio of the serial run time vs parallel run time[16]. The calculation is performed on a HP-Z620 workstation and each processor has a speed of 2.3 GHz.

Table 1 Grid scale and parallel computation efficiency

Element number	Processor number	Computation time/s	Parallel efficiency/%
20 000	1	63 510.940	—
20 000	2	35 853.529	88.57
20 000	4	20 649.937	76.89
20 000	8	11 321.835	70.12
12 800	1	60 187.588	—
12 800	2	34 738.309	86.63
12 800	4	20 251.545	74.30
12 800	8	11 364.728	66.20

2 Time Dependent Aerodynamic Module

2.1 Governing equation for fluid dynamic

The governing equation for the unsteady fluid dynamic model is

$$\iiint \frac{\partial W}{\partial t}\mathrm{d}\Omega + \Gamma\iiint \frac{\partial Q}{\partial \tau}\mathrm{d}\Omega +$$

$$\iint_{\partial\Omega}[F-G]\,\mathrm{d}S=0 \tag{6}$$

where Ω is the spatial domain for an arbitrary control volume and S its boundary, W the conservative quantities, Q the primitive variables, $\boldsymbol{\Gamma}$ the Weiss-Smith[20] preconditioning matrix which can accelerate the convergence speed for the flow solver at low speeds. F and G are the convective flux and viscous flux, respectively.

2.2 Time-integration scheme of fluid module

The dual time stepping scheme is employed to provide time-accurate solution of unsteady parachute aerodynamic simulation

$$\left[\frac{\Gamma}{\Delta\tau}+\frac{3}{2\Delta t}\frac{\partial W}{\partial Q}\right]\Delta Q\Omega^{t+\Delta t}=-\sum_{m=1}^{N_{\text{face}}}(F_m-G_m)S-\frac{(3W_m^{t+\Delta t}\Omega^{t+\Delta t}-4W^t\Omega^t+W^{t-\Delta t}\Omega^{t-\Delta t})}{2\Delta t} \tag{7}$$

where m is stage counter of pseudo time iteration, and N_{face} the face number of a control volume. The updating of primitive variables of pseudo time iteration is based on the preconditioned LU-SGS algorithm. The parallel computation strategy of the flow simulation only needs one operating level because only the flow field information of those control volumes near each logical boundaries need to be exchanged among processors. A compatible mesh is generated for the aerodynamic simulation based on the membrane structural mesh on canopy surface.

3 Automatic Mesh Deformation Module

The parachute fluid mesh is treated as a pseudo solid body[21] to transform with the large deformation of parachute canopy. The pseudo equilibrium equation governing this dynamic mesh algorithm is

$$\iiint_{\Omega}\boldsymbol{B}^{\mathrm{T}}\cdot\boldsymbol{D}\cdot\boldsymbol{B}\cdot\boldsymbol{U}\mathrm{d}\Omega=0 \tag{8}$$

where $\boldsymbol{B}^{\mathrm{T}}\cdot\boldsymbol{D}\cdot\boldsymbol{B}$ is the pseudo strain tensor, here $\boldsymbol{B}$ and $\boldsymbol{D}$ are the shape function matrix, and material matrix respectively. The shape changes of the canopy are treated as the Dirichlet boundary conditions for the mesh moving solver and the new grid coordinates can be updated by the pseudo displacement vector $\boldsymbol{U}$. The parallel computation strategy of this mesh moving algorithm is similar with the structure solver because they both use GMRES algorithm to solve the resulting system equations.

4 Parallel Computation Procedure for Parachute FSI Simulation

There are two stages in the FSI simulation: The first stage is the pre-inflation stage which uses a stand-alone nonlinear structure dynamic module to simulate parachute inflation procedure until a fully plump inflated canopy configuration is formed. The second stage is the fluid-structure coupling procedure which couples the nonlinear structure dynamic solver with unsteady preconditioning solver to predict the parachute descent speed as well as parachute configurations. The coupling stage is demonstrated in Fig. 3.

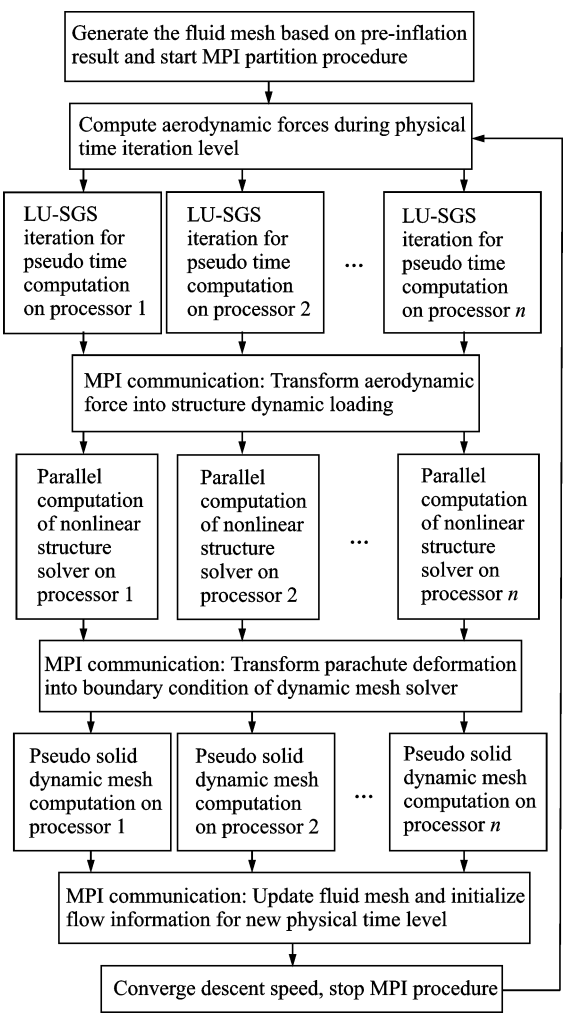

Fig. 3 Parallel computation procedure for ATPS parachute FSI simulation

5 ATPS Parachute FSI Simulation

5.1 ATPS parachute model and pre-inflation

The geometry parameters of the ATPS parachute are set according to Ref. [1] and demonstrated in Table 2. The initial unstressed state is demonstrated in Fig. 4(a). There are 28 suspension lines which are connected to 4 risers and the risers are connected to the payload. The payload is a point mass which has a mass of 100.697 5 kg[1]. The initial descent speed is 4.876 8 m/s[1] and the constant inflation-pressure is set to 14.567 2 Pa based on the evaluation of stagnation pressure.

Table 2 ATPS parachute geometrical parameter and material properties

Parameter	Value	Parameter	Value
Top width/m	6.431 28	Arm length/m	3.931 92
Stitching height/m	0.731 52	Bottom edge width/m	6.096 00
Riser lengt/m	1.219 20	Suspension line length/m	6.400 80
Membrane stiffness/Pa	$9.564\ 8\times10^{6}$	Membrane thickness/m	3.048×10^{-5}
Membrane density/(kg·m^{-3})	1 223.509 3	Cable stiffness/Pa	$5.342\ 0\times10^{8}$
Cable crossse-ctional area/m^2	3.11×10^{-6} m^2	Cable density/(kg·m^{-3})	1 223.509 32

This parachute structure model contains 55 987 nodes and 134 644 elements. Only the bottom node where the four risers join together is constrained as fixed boundary condition. The time step of nonlinear structural simulation is 5.0×10^{-4} s. After 6 000 nonlinear iterations, the parachute vibration becomes gradually stable, and the ATPS parachute pre-inflation results are demonstrated in Figs. 4 (b—e).

During the inflation stage, the impact energy of pressure loading transforms to unfolding energy and drives the four arms of parachute canopy to separate from the initial unstressed state (0.20 s). After the largest expanding motion (0.40 s), the fabric tension stress starts to spread in the remaining slack zone of parachute canopy (0.80 s), the fight between fabric expending inertia and

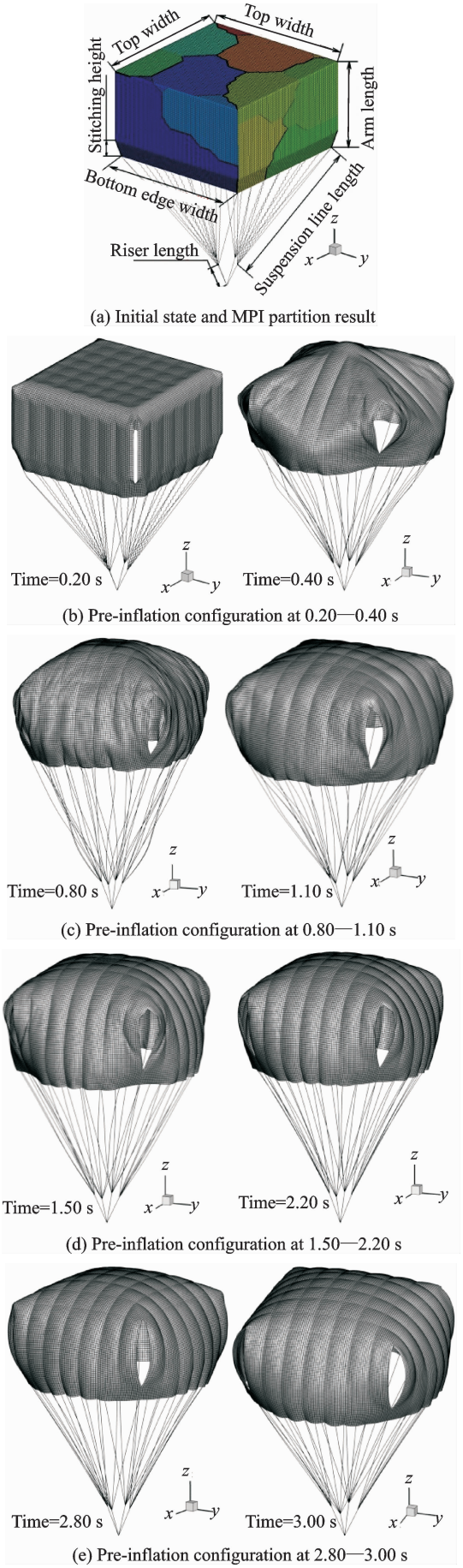

(a) Initial state and MPI partition result

(b) Pre-inflation configuration at 0.20—0.40 s

(c) Pre-inflation configuration at 0.80—1.10 s

(d) Pre-inflation configuration at 1.50—2.20 s

(e) Pre-inflation configuration at 2.80—3.00 s

Fig. 4 ATPS parachute pre-inflation simulation

tension stress transforms into the vibration of parachute membrane-cable system (Fig. 4 (c)). As the spreading speed of tension stress gradually catches up with the vibration spreading speed, a dynamic equilibrium state starts to form (Fig. 4 (d)) and the tension stress has changed the canopy shape into a relatively smooth inflated configuration(Fig. 4 (e)).

5.2 FSI simulation of parachute descent stage

A structural fluid mesh containing 3 860 439 hexahedral elements and 3 753 334 grid nodes is generated to conduct the numerical simulation of ATPS parachute aerodynamics (Fig. 5). During the FSI simulation of descent stage, the acceleration and descent speed in the vertical direction can be calculated by the one-degree free fall equations

$$\begin{cases} \ddot{u}_z^{t+\Delta t} = \dfrac{\rho V_\infty^2 A_r}{2} \cdot \dfrac{C_d^{t+\Delta t}}{m} - g \\ \dot{u}_z^{t+\Delta t} = \dot{u}_z^t + \ddot{u}_z^{t+\Delta t} \cdot \Delta t \end{cases} \tag{9}$$

where V_∞ and A_r represent initial free stream velocity and reference area, respectively. The reference area of ATPS parachute is set to 41.361 4 m^2 which is equal to the parachute canopy projected area of initial unstressed configuration (Fig. 4 (a)). C_d represents the drag coefficient, m the total mass of parachute-payload system. ρ and g are the air density and the gravity acceleration, respectively. The physical time step for the aerodynamic simulation is set to 5.0×10^{-3} s and the structural time step is 5.0×10^{-4} s. The FSI simulation of ATPS parachute is carried out on a PC-Cluster with 6 computation nodes and each node has 16 computation threads, the CPU type is Intel® Xeon® E5-2660. The physical time for parachute descent procedure is 5 s and there are 1 000 fluid physical time steps and 10 000 structural nonlinear iterations.

Fig. 6 demonstrates the flow fields of the FSI simulation results. During the FSI simulation of ATPS parachute descent stage, the shape changes of parachute system are smaller than the inflation stage, the breath vibration energy is separated and consumed by the tension stress near the four vents of parachute canopy, and finally reaches a dynamic equilibrium state. The amount of wrinkles are less than the inflation stage and the shape changes of canopy vents are also smaller than inflation stage, this is because the gradually balanced tension stress formed in inflation stage.

The flow structure can be separated into two main parts: One is the inner stream part which is prevented by parachute canopy and the other is the outer stream part which flow bypass the para-

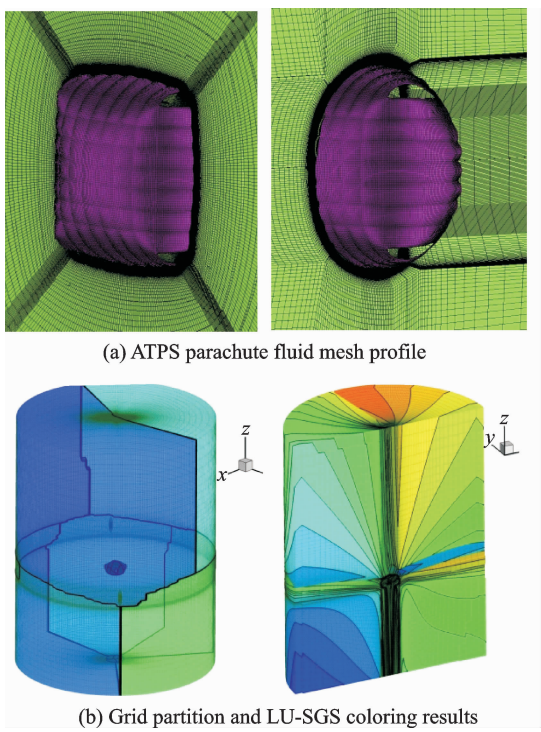

(a) ATPS parachute fluid mesh profile

(b) Grid partition and LU-SGS coloring results

Fig. 5 Fluid mesh of ATPS parachute

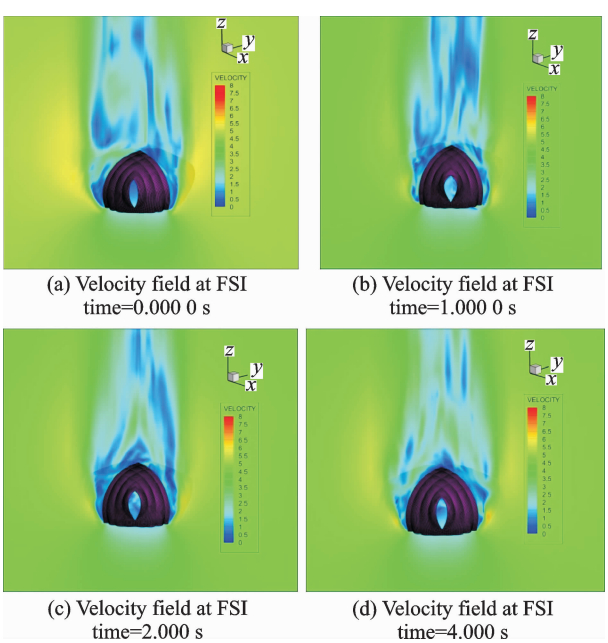

(a) Velocity field at FSI time=0.000 0 s

(b) Velocity field at FSI time=1.000 0 s

(c) Velocity field at FSI time=2.000 s

(d) Velocity field at FSI time=4.000 s

Fig. 6 Flowfields demonstration of FSI simulation

chute canopy. Because the inner stream cannot penetrate the inner surface of parachute canopy, the flow near the center vertical axis has to circle around and form two vortexes, this rotational motion causes an increase of air density and pressure near these areas (Fig. 7 (a)). On one hand, the dissipated kinetic energy during this procedure transforms into expanding energy of parachute canopy. On the other hand, caused by the viscous shearing force and the back flow near the bottom edge of parachute canopy, there forms two separate vortexes due to the rotatory inertia. As time advancing, the vortex position changes from their initial position, but the basic flow structure does not change (Fig. 7 (b)). Along with other smaller vortexes formed near parachute canopy, these special vortexes consists the basic structure of parachute flow field and the kinetic energy dissipation caused by this structure transforms into drag force for parachute system.

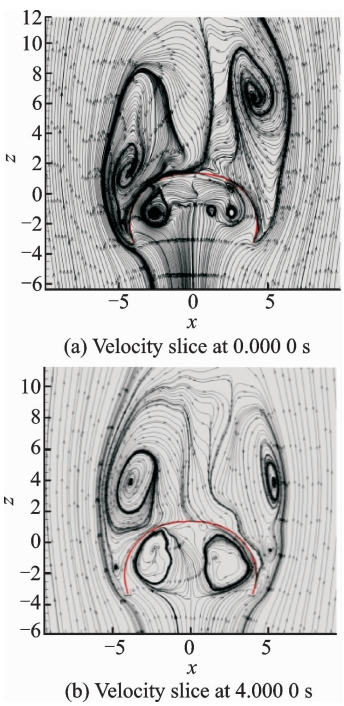

Fig. 7 Slice of parachute flowfield

Fig. 8 demonstrates the FSI simulation results of ATPS parachute descent speed compared with the results provided by Ref. [1]. The near steady descent speed in this paper and Ref. [1] is 4.693 92 m/s and 4.785 36 m/s, respectively. The changes of the descent speed are caused by the parachute breathe vibration which can be observed during the FSI simulation (Fig. 6).

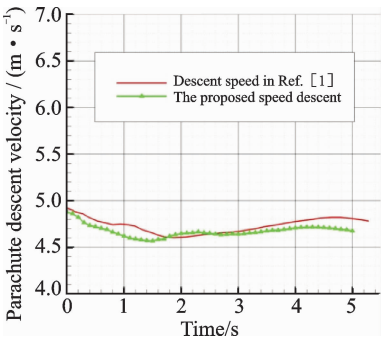

Fig. 8 FSI results of descent speed

6 Conclusions

The unsteady preconditioning method coupled with the nonlinear finite element algorithm is applied within MPI parallel computation environment to simulate the ATPS parachute transient dynamics. The FSI simulation of the ATPS parachute is carried out on a PC-Cluster and the result of descent speeds is compared with literature. The simulation result shows that the parachute flow field consists of complex vertex structure and the descent speed is affected by the breathe vibration. Apparently, there are some improvements needed for this parachute FSI simulation method:

(1) The wrinkles and contact problems during inflation stage need more robust dynamic mesh solver to extend the FSI simulation through entire parachute inflation stage.

(2) The aerodynamic force of the payload system needs to be computed and the six degree of freedom dynamic equation for the parachute-payload system needs to be studied to simulate the more complex descent problems with asymmetric flow conditions.

References:

[1] SATHE S, BENNEY R, STEIN K R, et al. Fluid-structure interaction modeling of complex parachute designs with the space-time finite element techniques [J]. Computers and Fluids, 2007, 36(1): 127-135.

[2] YU L, MING X. Study on transient aerodynamic characteristics of parachute opening process [J]. Ac-

ta Mechanica Sinica, 2007, 23(6): 627-633.

[3] ZHANG Hongying, LIU Weihua, QIN Fude, et al. Study on the canopy shape and the flow field during parachute inflation process [J]. Acta Aerodynamic Sinica, 2011, 29(3): 288-301. (in Chinese)

[4] BENNEY R J, STEIN K R. Computational fluid-structure interaction model for parachute inflation [J]. Journal of Aircraft, 1996, 33(4): 730-736.

[5] GUO Peng, XIA Gang, QIN Zizeng. Numerical simulation of parachute initial inflation phase based on control volume method[J]. Spacecraft Recovery and Remote Sensing, 2010, 31(6): 1-8. (in Chinese)

[6] KIM J D, LI Yan, LI Xiaolin. Simulation of parachute FSI using the front tracking method[J]. Journal of Fluids and Structures, 2013, 37: 100-119.

[7] STEINK R, TEZDUYAR T E, SATHE S, et al. Simulation of parachute dynamics during control line input operations [C]// 17th AIAA Aerodynamic Decelerator Systems Technology Conference and Seminar. Mouterey, CA: AIAA, 2003: 23-2151.

[8] STEIN K R, TEZDUYAR T E. Fluid-structure interaction of a round parachute: Modeling and simulation techniques [J]. Journal of Aircraft, 2001, 38 (5): 800-808.

[9] BAZILEVS Y, TAKIZAWA K, TEZDUYAR T E. Computational fluid-structure interaction, method and applications [M]. West Sussex, United Kingdom: John Wiley and Sons Ltd, 2013.

[10] STEIN K, BENNEY R, TEZDUYAR T E, et al. Parachute fluid-structure interactions: 3-D computation[J]. Computer Methods in Applied Mechanics and Engineering, 2000, 190(3): 373-386.

[11] TEZDUYAR T E, SATHE S. Modeling of fluid-structure interactions with the space-time finite elements: Solution techniques[J]. International Journal for numerical methods in fluids, 2007, 54(6/7/8): 855-900.

[12] STEINK, BENNEY R, TEZDUYAR T E, et al. Fluid-structure interactions of a cross parachute: numerical simulation [J]. Computer Methods in Applied Mechanics and Engineering, 2001, 191(6/7): 673-387.

[13] TAZDUYAR T E, OSAWA Y. Fluid-structure interaction of a parachute crossing the far wake of an aircraft[J]. Computer Methods in Applied Mechanics and Engineering, 2001, 191(6/7): 717-726.

[14] CHENG Han, YU Li, LI Shengquan. Numerical simulation of parachute inflation process based on ALE [J]. Journal of Nanjing University of Aeronautics and Astronautics, 2012, 44(3): 290-293. (in Chinese)

[15] CHENG Meng, WANG Lu, CHENG Han, et al. Numerical prediction analysis of parachute inflation process using fluid-structure interaction method [J]. Journal of Nanjing University of Aeronautics and Astronautics, 2013, 45(4): 515-520. (in Chinese)

[16] ZHANG Wenqing, ACCORSI M L, LEONARD J W. Parallel implementation of structural dynamic analysis for parachute simulation [J]. AIAA Journal, 2006, 44(7): 1419-1427.

[17] ACCORSI M, LEONARD J, BENNEY R, et al. Structure modeling of parachute dynamics [J]. AIAA Journal, 2000, 38(1): 139-146.

[18] LU K, ACCORSI M, LEONARD J. Finite element analysis of membrane wrinkling [J]. International Journal for Numerical Methods in Engineering, 2001, 50(5): 1017-1038.

[19] SAAD Y, SCHULTZ M H. GMRES: A generalized minimal residual algorithm for solving nonsymmetric linear systems [J]. Society for Industrial and Applied Mathematics, 1986, 7(3): 856-869.

[20] WEISS J M, SMITH W A. Preconditioning applied to variable and constant density time-accurate flows on unstructured meshes [C]// 25th AIAA Fluid Dynamic Conference. Colorado: AIAA, 1994.

[21] STEIN K, TEZDUYAR T E, BENNEY R. Mesh moving techniques for fluid structure interaction with large displacements[J]. Journal of Applied Mechanics, 2003, 70(1): 58-63.

Mr. **Fan Yuxin** is a doctoral candidate in College of Aerospace Engineering from Nanjing University of Aeronautics and Astronauticas, China. His research has focused on computational fluid dynamic and fluid-structure interaction method of parachute.

Prof. **Xia Jian** received his Ph. D. degree in College of Aerospace Engineering from Nanjing University of Aeronautics and Astronauticas, in 1998. From 2001 to 2003, he received his post doctor degree in University of Texas at Austin. From 2003 to present, he has been with College of Aerospace Engineering, Nanjing University of Aeronautics and Astronautics (NUAA), where he is currently a full professor and executive director of the Aerodynamic. His research has focused on computational fluid dynamic, which includes overset grid, DSMC method, parallel computation, fluid-structure interaction, multiphase flow.

(Executive Editor: Xu Chengting)